Developmental Cell
Article

Focal Defects in Single-Celled Tubes Mutant for *Cerebral Cavernous Malformation 3*, *GCKIII*, or *NSF2*

Yanjun Song,[1] Melissa Eng,[1,2] and Amin S. Ghabrial[1,*]
[1]Department of Cell and Developmental Biology, Perelman School of Medicine, BRBII/III Room 1214, 421 Curie Boulevard, University of Pennsylvania, Philadelphia, PA 19104, USA
[2]Present address: Department of Biology, University of Washington, Box 351800, Seattle, WA 98195-1800, USA
*Correspondence: ghabrial@mail.med.upenn.edu
http://dx.doi.org/10.1016/j.devcel.2013.05.002

SUMMARY

Tubes of differing cellular architecture connect into networks. In the *Drosophila* tracheal system, two tube types connect within single cells (terminal cells); however, the genes that mediate this interconnection are unknown. Here we characterize two genes that are essential for this process: *lotus*, required for maintaining a connection between the tubes, and *wheezy*, required to prevent local tube dilation. We find that *lotus* encodes N-ethylmaleimide sensitive factor 2 (NSF2), whereas *wheezy* encodes Germinal center kinase III (GCKIII). GCKIIIs are effectors of Cerebral cavernous malformation 3 (CCM3), a protein mutated in vascular disease. Depletion of *Ccm3* by RNA interference phenocopies *wheezy*; thus, CCM3 and GCKIII, which prevent capillary dilation in humans, prevent tube dilation in *Drosophila* trachea. Ectopic junctional and apical proteins are present in *wheezy* terminal cells, and we show that tube dilation is suppressed by reduction of NSF2, of the apical determinant Crumbs, or of septate junction protein Varicose.

INTRODUCTION

Most organs are composed of epithelial or endothelial cells organized as tubes; junctional complexes maintain the intercellular or autocellular connections ("seams") that seal the cells into selectively permeable tubes. Should these connections be compromised, the consequences for organ function can be catastrophic. For example, individuals with the vascular disease, familial cerebral cavernous malformation (CCM), may suffer from seizures and strokes as a consequence of dilated leaky tubes (Clatterbuck et al., 2001; Haasdijk et al., 2012; Rigamonti et al., 1988).

Three architecturally distinct tube types have been described (Lubarsky and Krasnow, 2003), and all three are found in the *Drosophila* tracheal system. These include multicellular seamed tubes (with intercellular junctions), seamed tubes formed by single cells (with autocellular junctions), and seamless tubes formed within single cells (no junctions) (Ribeiro et al., 2004; Samakovlis et al., 1996a) (Figure 1A). Most seamless tubes are thought to form intracellularly, although they may also form by fusion of membrane along autocellular junctions, converting autocellular tubes into seamless ones (Lubarsky and Krasnow, 2003; Rasmussen et al., 2008; Stone et al., 2009).

Tubes with single seams (autocellular) and seamless tubes form relatively late during tracheal development. The first tubes of the tracheal system are large multicellular sacs generated by invagination from the embryonic ectoderm. The tracheal epithelial cells are polarized along their apical-basolateral axis, with the apical membrane of each cell facing the lumen of the tracheal sac to which it belongs. Cells are next recruited to the distinct primary branches that migrate away from the sacs toward Branchless-FGF chemoattractant cues (Sutherland et al., 1996). Many of the primary branches initially form short wide tubes that lengthen and narrow over time, as the cells that comprise them intercalate, changing the underlying tubular architecture from multicellular to autocellular (Ribeiro et al., 2004). Tip cells are required for, and lead, the migration of the new branches (Ghabrial and Krasnow, 2006). Ultimately, tip cells assume specialized cell fates (terminal cell or fusion cell), and initiate secondary branch formation by targeting apical membrane internally to form seamless tube (Gervais and Casanova, 2010; Gervais et al., 2012; Ikeya and Hayashi, 1999; Lee and Kolodziej, 2002; Llimargas, 1999; Samakovlis et al., 1996a, 1996b). The precise mechanism by which this occurs remains subject to debate and may differ between terminal and fusion cells (Gervais and Casanova, 2010; Lubarsky and Krasnow, 2003; Schottenfeld-Roames and Ghabrial, 2012; Uv et al., 2003).

Intriguingly, *Drosophila* terminal cells contain both autocellular and seamless tubes (Samakovlis et al., 1996a, but see also Gervais and Casanova, 2010). Transition from one tube type (autocellular) to the other (seamless) occurs within the terminal cell at a location proximal to the terminal cell nucleus (Figure 1B). This observation raises a number of questions including: how do the two tube types connect to each other, how do they match each other in diameter, and which pathways are required to regulate and execute these processes? To begin to address these questions, we have taken a genetic approach and have screened through a large collection of terminal cell mutants (Ghabrial et al., 2011) to identify those that display tube morphogenesis defects within the region of the terminal cell wherein the autocellular-to-seamless tube transition occurs (hereafter, the "transition zone").

Here we report the identification and characterization of two mutants that disrupt lumen morphology in the transition zone in strikingly different ways. The first mutant, *lotus*, shows a transition zone gap in gas-filled tube, and more precise analysis shows that the gap corresponds to a local absence of tube, although tube is present proximal and distal to the gap. The second mutant, *wheezy*, shows dramatic tube dilation in the transition zone. These mutants may thus have opposing effects on the addition of apical membrane within the transition zone: too little, resulting in a gap, in *lotus* mutants; and too much, resulting in a dilation, in *wheezy* mutants. We show that *lotus* encodes N-ethylmaleimide sensitive factor 2 (NSF2), a protein required for SNARE recycling (Zhao et al., 2012). This implies an especially stringent requirement for vesicle traffic in connecting the two tube types. Significantly, we find that the second mutant, *wheezy*, encodes Germinal center kinase III (GCKIII). The human orthologs of GCKIII are effectors of the protein encoded by the human vascular disease gene, *Cerebral cavernous malformation 3* (*Ccm3*), and are putative Golgi-resident kinases (Fidalgo et al., 2010). Patients suffering from cerebral cavernous malformations show gross dilations of cerebral capillaries, thus suggesting that CCM3/GCKIII play a conserved role in tubulogenesis in limiting diametric tube expansion. Mutations in *lotus* and in *wheezy* both point to a crucial role of apical membrane delivery in tube morphogenesis.

We next go on to show that *Drosophila Ccm3* has a loss of function phenotype identical to *GckIII*, and that it interacts genetically with *GckIII*. Interestingly, our results stand in contrast to a previous report suggesting a requirement for the genes in tracheal lumen formation (Chan et al., 2011). Further, we find ectopic localization of junctional proteins in *Ccm3*-depleted or *GckIII* mutant cells, and an overaccumulation of the apical determinant, Crumbs, in *GckIII* mutant cells. In contrast, although Crumbs also accumulates in *lotus*/*Nsf2* mutant cells, it does not appear to be enriched in the lumenal membrane. Overexpression of Crumbs by itself induces formation of multiple tiny dilations throughout the terminal cell, but not a large transition zone tube dilation. Nevertheless, knockdown of *crumbs* in *GckIII* mutants strongly suppresses the large local dilation defect. Similarly, we find that mutations in *lotus* (*Nsf2*), that cause mislocalization of Crumbs, are epistatic to *GckIII*. We also find that knockdown of the essential septate junction scaffold, Varicose (a MAGUK protein orthologous to human PALS-2), suppresses the transition zone dilation defect associated with *GckIII* mutants. These data suggest that it is the inappropriate increase of septate junctions in combination with overaccumulation of Crumbs that confers a transition zone dilation defect. These studies of transition zone tube morphogenesis have direct relevance to human development and disease, and provide important mechanistic insight into the basic biological question of how tubes of differing architecture connect to each other.

RESULTS

Two Mutants Affect Tube Morphology in the Transition Zone

In a collection of mutants that nearly saturates the third chromosome for tracheal morphogenesis genes (Ghabrial et al., 2011), we were able to identify only two loci with transition zone-specific terminal cell tubulogenesis defects. Terminal cells mutant for *lotus* displayed a gap in the gas-filled transition zone tube (compare Figures 1C–1C″ and 1D with 1E–1E″ and 1F; for other *lotus* phenotypes, see Figure S1 available online) (Ghabrial et al., 2011). In contrast, terminal cells mutant for *wheezy* displayed a transition zone tube dilation defect (Figures 1G–1G″ and 1H; for other *wheezy* phenotypes see Figure S1).

lotus Encodes *Drosophila* NSF2

Mapping of *lotus* (Figure 2A; Experimental Procedures) defined a 180 kb interval that included only seven candidate genes: *art9*, *art6*, *CG14362*, *CG31495*, *Mst87F*, *Nsf2*, and *e5*. We sequenced these on *lotus* mutant chromosomes and identified single point mutations for each allele of *lotus* in the N-ethylmaleimide sensitive factor 2 (NSF2) primary transcript; these resulted in predicted missense (*312*, *B91*) and nonsense mutations (*O48*) as well as a splice donor mutation (*urdur2*) (Figure 2B). We confirmed gene identity by testing the ability of terminal cell-specific RNAi knockdown of *Nsf2* to phenocopy *lotus* (Figures 2C–2D′; 52% of terminal cells showed a gap defect, n = 80). *Drosophila* has two NSF orthologs, with NSF1 being neuron-specific (Golby et al., 2001; Sanyal and Krishnan, 2001). NSF is an AAA protein required for SNARE recycling, and therefore ought to affect all aspects of SNARE-dependent transport, but surprisingly shows an uncommon and specific transition zone defect in terminal cells.

Characterization of the Transition Zone in *lotus* Terminal Cells

The phenotype of *lotus* transition zone tubes could reflect a defect in gas-filling for that portion of the tube, or absence of the tube. In this context, it should be noted that tracheal tubes are thought to gas-fill by forcing dissolved gas out of solution (Tsarouhas et al., 2007). Thus, discontinuous isolated tubes in terminal cells could be gas-filled even in the absence of a physical connection that would allow diffusion from the external environment. Further complicating the analysis, we found that although 35% of $lotus^{O48}$ terminal cells displayed the gap defect described above, the remaining 65% of cells lacked gas-filling in all terminal cell tubes (n = 20). We examined homozygous mutant *lotus* first instar larvae, and found that the initial formation and gas-filling of the terminal cell tubes occurred normally (Figure S4). We next asked whether the defect is in maintenance of gas-filling, maintenance of tube connectivity, or both. In control wild-type clones in third instar larvae, a GFP-excluding lumen could be detected; therefore we asked if tubes could be detected in *lotus* cells by GFP exclusion, and also assayed for the presence of tube using a marker of terminal cell lumenal membrane (α-Wkdpep) (Schottenfeld-Roames and Ghabrial, 2012) (Figures 2E–2F′). We found that ~70% of $lotus^{O48}$ mutant terminal cells show a discontinuous tube that is disrupted in the transition zone (n = 13). These data suggested that tube in the transition zone is uniquely sensitive to defects in vesicle trafficking, indicating a key role for membrane fusion in the maintenance of a connection between seamed and seamless tubes, as

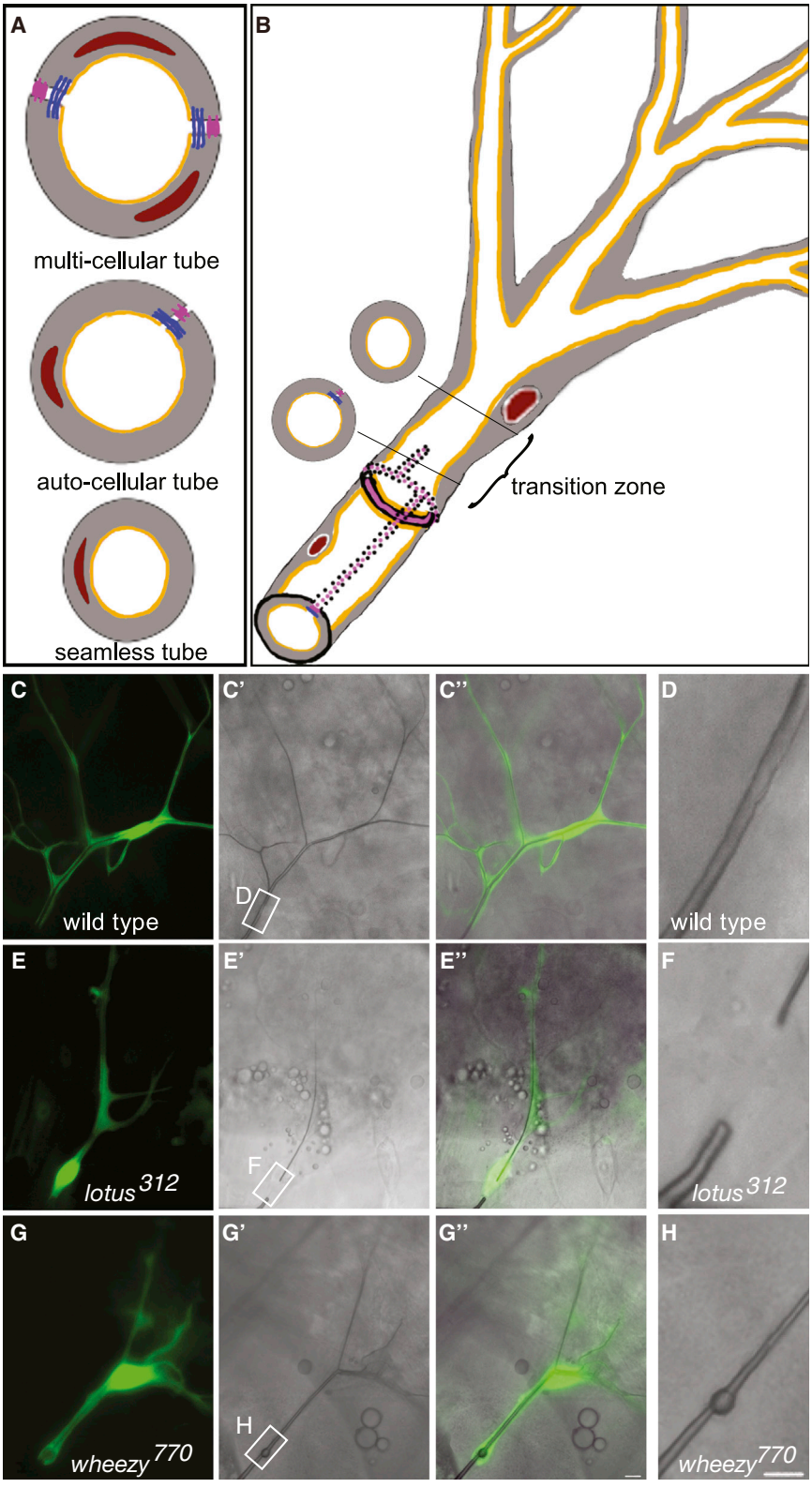

Figure 1. Identification of Mutants with Tube Defects in the Terminal Cell Transition Zone

(A and B) Three distinct tube architectures (A) are found in the tracheal system. Multicellular tubes (top panel; two to five cells around the circumference of the tube; adherens junctions, blue; septate junctions, magenta; nuclei, brick red; cytoplasm, gray; apical membrane, mustard) are found along the dorsal trunks of the tracheal system, whereas single cells make the autocellular tubes (middle panel) that comprise most primary tracheal branches, and intracellular seamless tubes (bottom panel) are found in the cells that make secondary and tertiary tracheal branches. Terminal cells (B) mark the ends of the tracheal tubes. They are connected via intercellular junctions to a stalk cell. A line of junctional staining stretches from the intercellular junction into the terminal cell, suggesting that the proximal part of the terminal cell tube is autocellular. A transition from autocellular to seamless occurs at a variable position between the intercellular junction and the terminal cell nucleus (red). We refer to this region of the terminal cell as the transition zone.

(C–H) Micrographs of positively marked (GFP, green) homozygous tracheal clones in terminal cell positions are shown in third instar larvae. In control clones (C and D), a terminal cell with multiple cellular extensions (C), contains gas-filled tubes (C′); refraction of light reveals the gas-filling state in bright-field microscopy. In a merged image (C″), it is apparent that single gas-filled tubes are present in each cellular extension. The rectangular box in (C′) marks the transition zone, shown at higher magnification in (D). (D) A smooth gas-filled tube is detected with no obvious difference in morphology marking the junction of seamed and seamless tubes. In *lotus* mutant clones (E and F), terminal cells are smaller with fewer branches and exhibit a gas-filling gap within the transition zone. In *wheezy* mutant clones (G and H), a single large dilation is detected within the tube of the transition zone. (C–H) Montages assembled from multiple z slices. Scale bars represent 5 μm.

See also Figure S1.

well as in their gas-filling. The affected trafficking events may be those for which one or more required SNARE proteins are especially limiting.

wheezy Encodes the *Drosophila* Germinal Center Kinase III

Complementation tests against overlapping chromosomal deficiency strains defined a *wheezy* candidate interval spanning ~50 genes (Figure 3A). Of these candidate genes, *GckIII* was of particular interest because of the vascular defects associated with the vertebrate orthologs (Zheng et al., 2010), and because of the reported Golgi localization of GCKIII (Preisinger et al., 2004), which would be consistent with a role in regulation of vesicle trafficking, a process our recent data suggest to be critical to seamless tube morphogenesis (Schottenfeld-Roames and Ghabrial, 2012). The *GckIII* gene was sequenced, and the

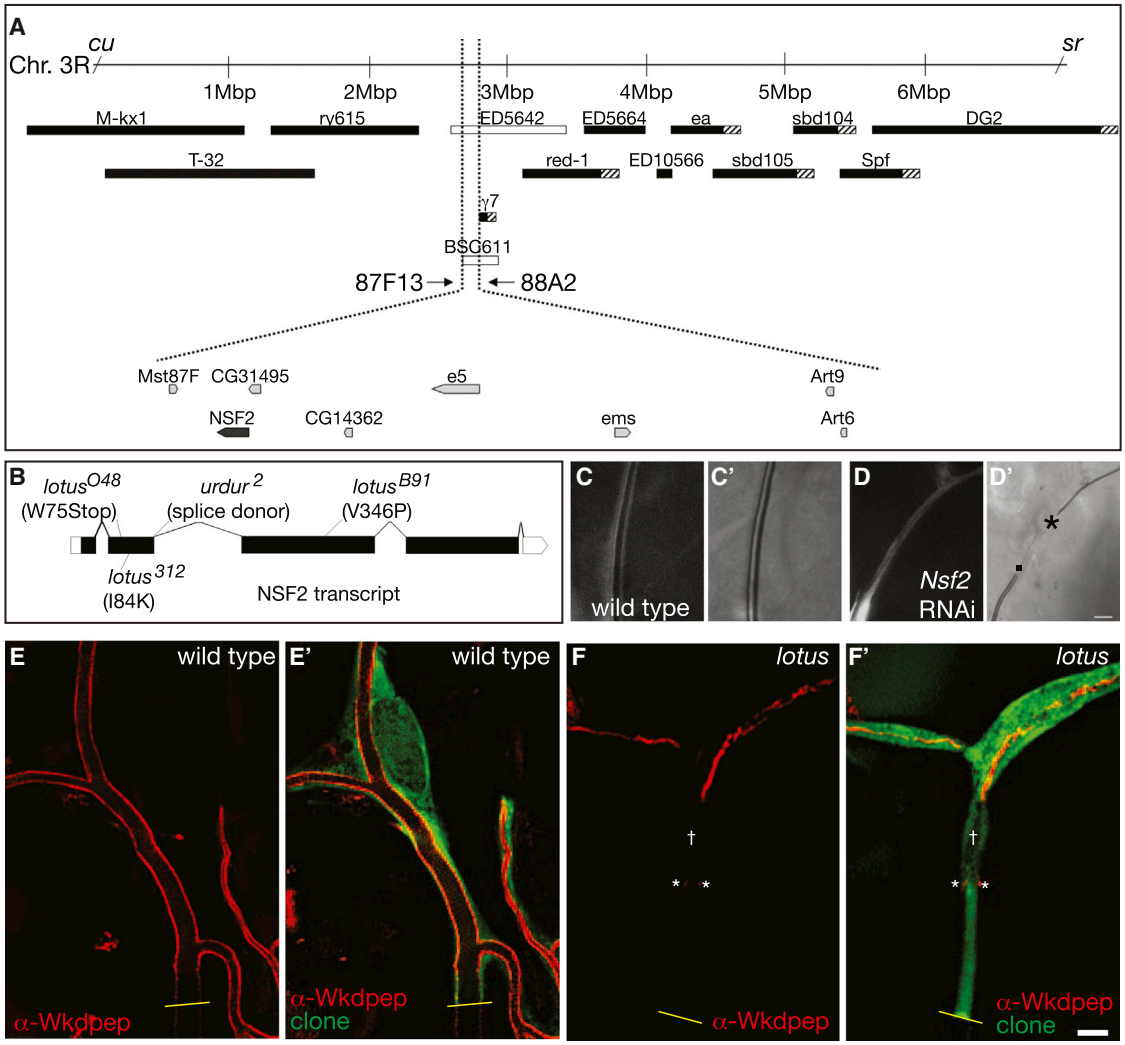

Figure 2. The Cloning and Phenotypic Characterization of *lotus*

Meiotic recombination mapping placed *lotus* between the visible recessive markers *curled* (*cu*) and *stripe* (*sr*) on the right arm of the third chromosome (A). Complementation tests against an overlapping set of chromosomal deletions (black boxes indicate the cytological extent of the deletion in strains that complement, white boxes strains that uncover; hashed boxes indicate regions of ambiguity in the deletion breakpoint) defined a *lotus* candidate region between 87F13 and 88A2. Mutations in *urdur* map to this region, and fail to complement *lotus*. However, the molecular identity of *urdur* was unknown. We analyzed the eight genes in the candidate region and identified single nucleotide changes in *Nsf2* (B) for all of the alleles of *lotus* and *urdur* examined. The $lotus^{O48}$ allele is predicted to be a molecular null allele of *Nsf2*, and was used hereafter for the phenotypic analysis of *lotus*. We were able to confirm the identity of *lotus* by phenocopying the third instar transition zone gap defect by specifically knocking down *Nsf2* with pantracheal RNAi (compare C and C′ with D and D′). In (C) and (D) the cytoplasm of the terminal cell transition zone is shown, whereas in (C′) and (D′) the corresponding bright-field image reveals the presence or absence of gas-filled tube. (D′) A period marks the stalk cell proximal portion of the terminal cell transition zone lack gas-filled tube, whereas the asterisk marks the resumption of gas-filled tube at the distal end of the transition zone. We note that the cell size and tube diameter of *lotus* mutants is severely reduced as compared to wild-type—this aspect of the RNAi phenotype is also readily visible in homozygous mutant cells as compared to wild-type (compare E with F). To examine the transition zone tube at higher resolution, mosaic third instar larvae were filleted, fixed, and stained with anti-GFP antibodies (green) to identify mutant clones and with α-Wkdpep antibodies (red) to mark the lumenal membrane. Images were deconvolved using Leica software. In control wild-type clones (E and E′), lumenal membrane staining in the transition zone is uninterrupted (although the level tapers off toward the junction with the stalk cell, junction with stalk cell is marked with a yellow line). In contrast, in *lotus* mutant clones (F and F′) lumenal staining is not continuous. In some instances (as shown), staining reveals a tube that begins several microns distant from the point (yellow line) at which the terminal cell contacts the neighboring stalk cell, whereas at other times tube extended from the stalk cell junction a few microns into the terminal cell (not shown), before ending only to resume more distally. We also note a region of several microns in which a lumenal space (†) appears to be detected by exclusion of GFP, but which lack α-Wkdpep staining. Interestingly puncta of lumenal membrane staining (*) are present at the proximal end of this region, perhaps suggestive of tube loss or of a deficit in tube growth relative to the increase in terminal cell size. Smaller areas of tube discontinuities could also be discerned at other positions in the terminal cell. (E–F′) Montages assembled from multiple z slices. Scale bars represent 5 μm.

See also Figure S4.

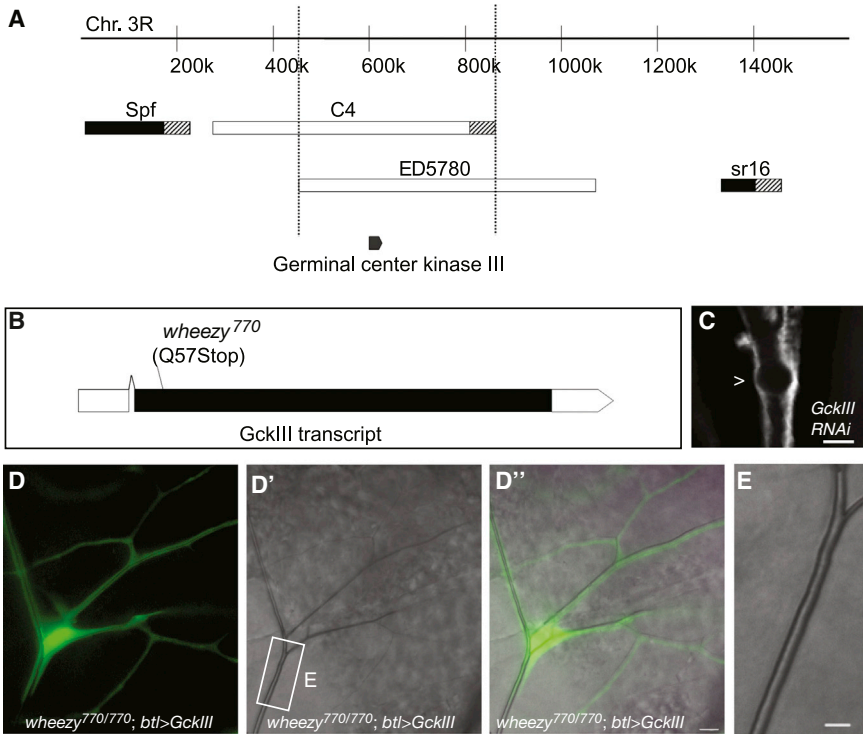

Figure 3. Molecular Identification of *wheezy* and Transgene Rescue

Complementation tests against overlapping chromosomal deletion strains spanning the right arm of the third chromosome were carried out to map *wheezy*. Two partially overlapping deficiency strains—Df(3R)C4 and Df(3R) ED5780—uncovered *wheezy*. Within the ~400 kb region defined by the deletion breakpoints, we identified *germinal center kinase III* (*GckIII*), as a likely candidate. Upon sequence analysis, *wheezy* was found to have a single nucleotide change in the GCKIII coding sequence that introduces an early stop (B). We expect that the *wheezy*^{770} allele is molecularly null for *GckIII*, because the encoded protein would be truncated after 56 amino acids and would therefore lack a kinase domain. Pan-tracheal RNAi knockdown of GCKIII was able to phenocopy the *wheezy* transition zone tube dilation (C, dilation marked with >). A UAS-*wheezy* transgene generated using a wild-type *GckIII* cDNA rescued the *wheezy* mutant phenotype upon pan-tracheal expression (D and E). (D) Shows a fluorescent image of a positively marked (GFP, green) *wheezy* mutant terminal cell clone that is also expressing a wild-type *GckIII* transgene under control of the *breathless*-GAL4 driver. (D′) Shows the bright-field image of the same clone and (D″) shows a merged image. The terminal cell transition zone (from stalk cell:terminal cell interface to terminal cell nucleus, white rectangle) looks normal. In (E), the transition zone (indicated by rectangle in D′) is shown enlarged; note the absence of the dilation defect characteristic of *wheezy* mutant terminal cells. All images depict third instar larvae. (D-E) Montages assembled from multiple z slices. Scale bars represent 5 μm.
See also Figure S3 and Table S1.

wheezy^{770} allele was found to be a molecular null for GCKIII, as we identified a nonsense mutation predicted to terminate the protein after 56 amino acids (Figure 3B). We confirmed gene identity by recapitulating the *wheezy* mutant phenotype (Figure 3C; Table S1) in a substantial fraction of terminal cells with pan-tracheal knockdown of GCKIII. As was true in our mosaic analysis with *wheezy*, only terminal cells showed *GckIII* RNAi-induced defects (data not shown). Although the most prominent defect (and the focus of our studies) was the transition zone tube dilation, we did note additional terminal cell defects consistent with a general effect on the lumenal membrane (as described in Figure S1). In a final proof that *wheezy* encodes *Drosophila* GCKIII, we were able to rescue all tracheal defects observed in *wheezy* mutants with tracheal-specific expression of a wild-type *GckIII* cDNA (Figures 3D and 3E).

Knockdown of *Drosophila Ccm3* (CG5073) Phenocopies *wheezy*

The three vertebrate GCKIII family members (Mst4, Stk24, Stk25) bind in vitro to Cerebral cavernous malformation 3 (CCM3/PDCD10) (Voss et al., 2009; Zheng et al., 2010). Mutations in *Ccm3* are causative for a vascular disease in humans characterized by gross dilation of cerebral capillaries, and CCM3 has been shown to have an essential role in endothelial cells for normal vascular development (Bergametti et al., 2005; Chan et al., 2011; Guclu et al., 2005; He et al., 2010; Lee et al., 2008; Pagenstecher et al., 2009; Voss et al., 2009). Although human disease has not been linked to mutations in GCKIII proteins, knockdown of multiple *stk24* and *stk25* family members in zebrafish (Zheng et al., 2010) conferred cardiovascular defects identical to those seen with knockdown of both zebrafish CCM3 orthologs (Voss et al., 2009). Because CCM3 is well conserved in *Drosophila* (Figure 4A), and the *Drosophila* CCM3 and GCKIII proteins bind (Chan et al., 2011), we sought to determine whether loss of Ccm3 would phenocopy *wheezy* or show the lumenization defect previously reported in the tracheal system for RNAi of *GckIII* and *Ccm3* (Chan et al., 2011). Indeed, we found that pan-tracheal knockdown of *Ccm3* caused transition zone tube dilation (Figure 4B; Table S1). We note that the *Ccm3* dilation is somewhat less extensive than that seen with *GckIII*, this could reflect a maternal contribution of *Ccm3* or incompleteness of knockdown. We next tested for genetic interactions between *wheezy* (*GckIII*) and *Ccm3* using a chromosomal deletion for *Ccm3* (Df(3R)EXEL6174; for convenience, referred to here as *Ccm3*^{DF}), as well as *Ccm3* alleles we generated by mobilization of a P element in the gene (P{EPg}CG5073^{HP36555}; Experimental Procedures; Figure 4C). We found that heterozygosity for *Ccm3* enhanced the penetrance of the *GckIII* RNAi phenotype, and that heterozygosity for *wheezy* likewise enhanced the penetrance of the *Ccm3* RNAi phenotype (Figures 4D and 4E). Together, these data demonstrate conservation of the CCM3-GCKIII pathway in tube morphogenesis between flies and man.

How loss of CCM3 or GCKIII activity causes a tube dilation defect has not been clear. It has been suggested that phosphorylation of Moesin may be the key event downstream of GCKIII kinase activity in endothelial cells (Zheng et al., 2010);

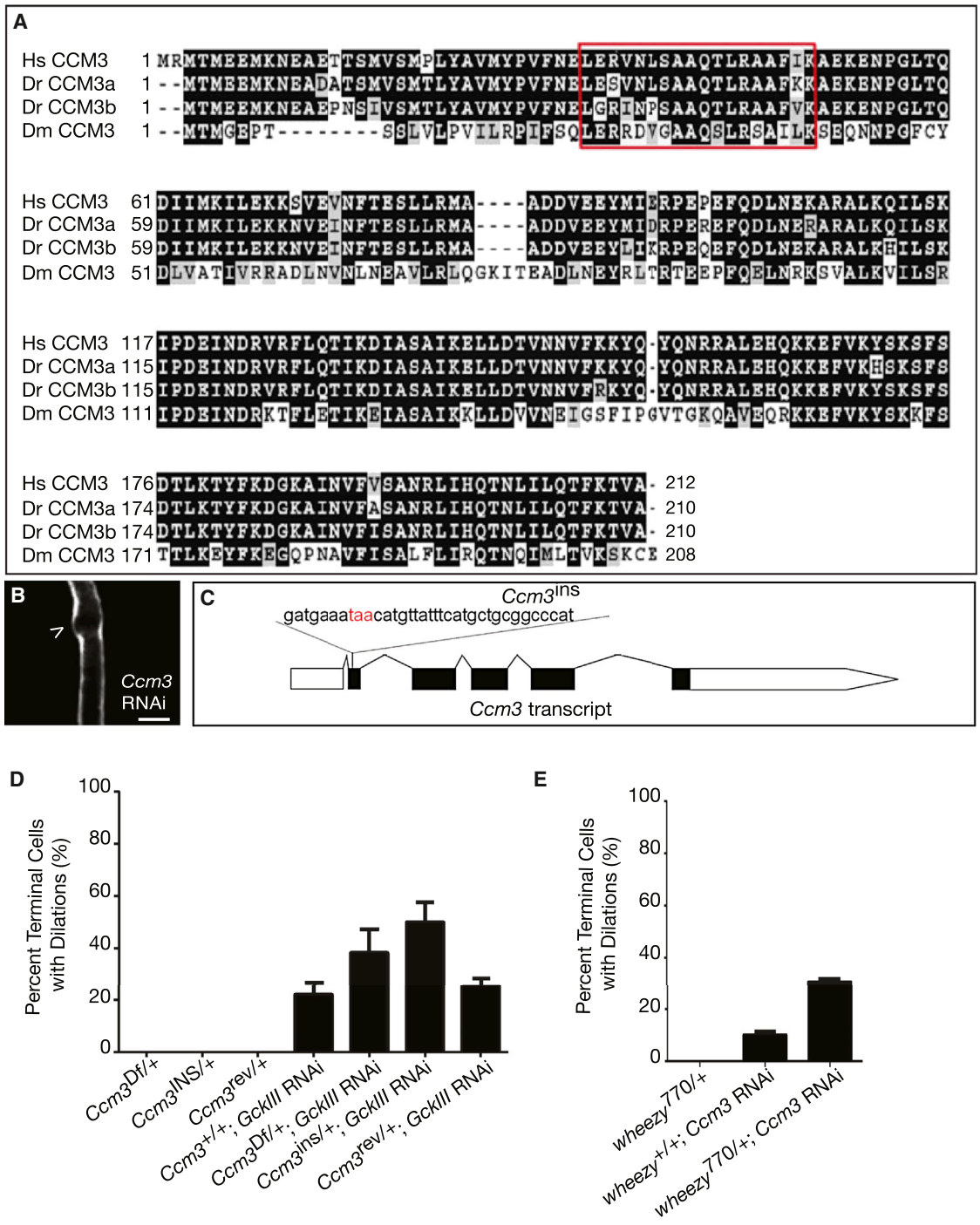

Figure 4. *Ccm3* Knockdown and *GckIII*/*Ccm3* Genetic Interaction

The *Drosophila* genome contains a single well-conserved (47% identity, 67% similarity) CCM3 ortholog (A). A stretch of 18 amino acids (red box) identified as essential for interaction with GCKIII (Voss et al., 2009) shows 56% identity and 72% similarity to the human protein. Pan-tracheal knockdown of *Ccm3* conferred a transition zone tube dilation defect very similar to that seen with loss of GCKIII activity (B, transition zone dilation indicated by >). A strain with a P element insertion in the second exon of *Ccm3* was obtained. The P element was mobilized and two derivatives were recovered: (C) $Ccm3^{ins}$, in which P element excision left behind a small insertion introducing extraneous coding sequence and an in-frame stop codon; and $Ccm3^{rev}$, a precise excision (*rev*ertant) of the P element. Both of these derivatives retain lethal mutations elsewhere on the right arm of chromosome 3. We tested the ability of these alleles to enhance the penetrance of the *GckIII* RNAi tube dilation (D). Conversely, mutation of a single copy of *GckIII* was tested for the ability to enhance the penetrance of the *Ccm3* RNAi tube dilation (E). None of the chromosomes tested displayed a haploinsufficient transition zone defect. The mean of three trials ± SEM are shown in (D) and (E). All larvae were scored at third instar. Scale bar represent 5 μm.

See also Figure S3 and Table S1.

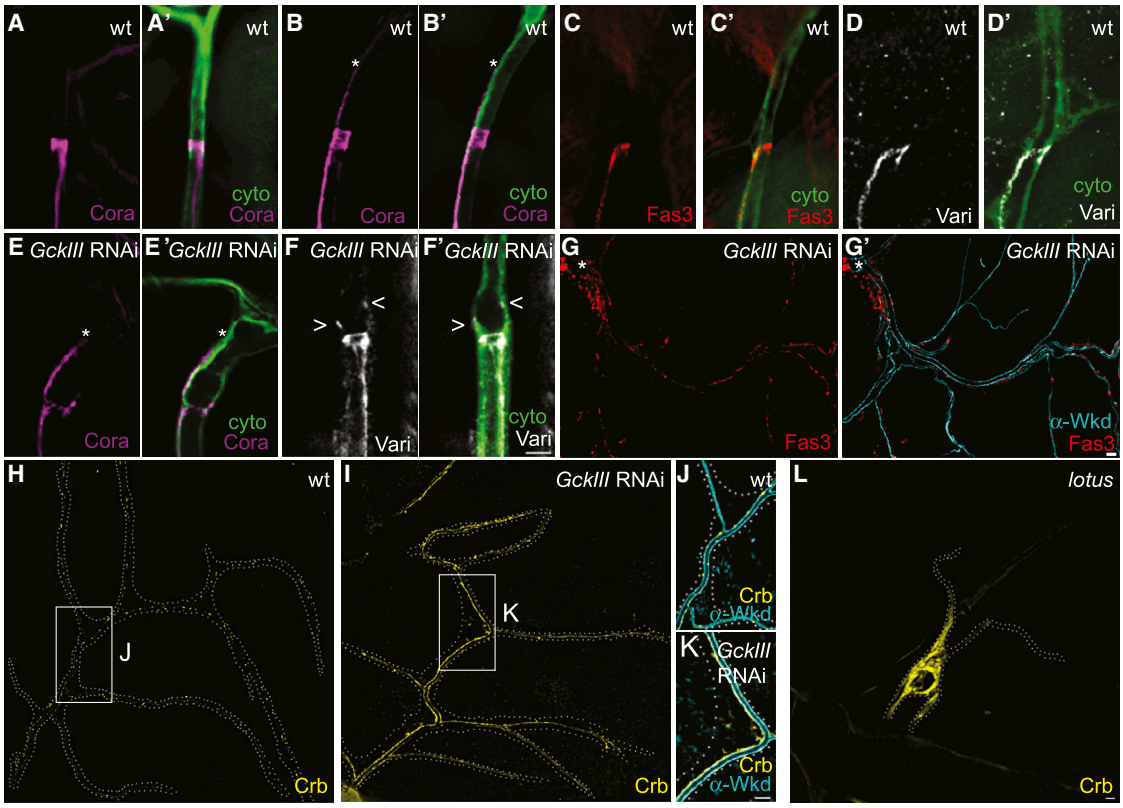

Figure 5. Ectopic Septate Junctions and Apical Membrane in *wheezy* Mutant Cells

We examined the distribution of septate junction proteins in wild-type terminal cells (A–D′), and in terminal cells in which *GckIII* had been knocked down by RNAi (E–G′). We found that in the vast majority of terminal cells, septate junctions do not extend into the terminal cell (A, C, and D); however, in ~4% of terminal cells a line of septate junctions extending into the terminal cell toward nucleus, similar to that reported for embryonic terminal cells, was detected (asterisk marks the end of a line of septate junction staining extending into the terminal cell in B and B′). This pattern of staining was observed with Coracle (magenta), Fas3 (red), and Varicose (white). In *GckIII* RNAi terminal cells showing a dilation defect, a line of septate junction staining (asterisk as in B) was detected extending into the cells (E and E′) at frequency almost an order of magnitude higher than wild-type. Additional terminal cells displayed punctate septate junction staining (marked by < and > in F and F′). Last, short discontinuous patches of septate junction could be observed 10 s or 100 s of microns away from the transition zone (G and G′; asterisk marks the transition zone dilation—upper left corner). (G′) Fas3 puncta appeared present at the basolateral membrane, rather than at the apical membrane marked by α-Wkd staining (cyan). (H) Discrete puncta of Crumbs decorated the lumenal membrane of wild-type terminal cells, but in *GckIII*-depleted (RNAi) terminal cells (I), Crumbs levels appeared elevated and its distribution altered to more evenly coat the lumenal membrane (J and K, corresponding to areas marked by white rectangles in H and I, respectively). In *lotus* mutant terminal cell clones (L), in contrast, Crumbs no long appeared restricted to the lumenal membrane. For (H–L), cell outlines (white dots) were traced and superimposed on the fluorescent images. All images depict third instar larvae. (A–B′, E–G′, and L) Montages assembled from multiple z slices.Scale bars represent 5 μm.
See also Figure S5.

we therefore sought to determine whether *moesin* played a key role in *wheezy* transition zone tube dilation. First, we found that *moesin* loss of function does not affect transition zone tube in an otherwise wild-type background (data not shown). Second, expression of a phosphomimetic isoform of Moesin in *GckIII* mutant terminal cells does not suppress the transition zone tube dilation (data not shown). Last, in mosaic larvae, we found that phospho-Moesin levels appear to be substantially higher in *wheezy* mutant terminal cells than in neighboring heterozygous cells, the opposite of the expected outcome were Moesin a target of GCKIII kinase activity (Figure S2). Interestingly, p-Moe appears to be especially enriched in the transition zone, in association with dilated tube (45%, n = 11). These data are consistent with published results that Slik is the Ste20K responsible for phosphorylation of Moesin in epithelia (Hughes et al., 2010), and lead us to look elsewhere for candidate GCKIII substrates.

Defects in the Abundance and Localization of Junctional and Apical Proteins

In the embryonic tracheal system, septate junctions (functional equivalent to vertebrate tight junctions) have been suggested to line the intercellular connection between the terminal cell and its neighboring stalk cell, and also to extend in from the intercellular junction into the terminal cell transition zone (Samakovlis et al., 1996a). Because of the transition zone defects of *lotus* and *wheezy*, we wished to determine whether the transition zone junctions were perturbed. In contrast to our expectations, we found that in wild-type third instar larvae (Figures 5A–5D′), septate junctions extended into the transition

zone of only ~4% of terminal cells (n = 49). We interpret this outcome as suggesting that a remodeling of the junctional complexes had occurred during development. When we went on to examine terminal cells depleted of *GckIII* by RNAi, we found septate junctions appeared to extend into the transition zone at a much higher frequency than in wild-type (Figures 5E and 5E′)—32% by varicose staining (n = 25) and 42% by Fas3 (n = 64) or Coracle (n = 45) staining, with patchy punctate junctional staining (Figures 5F and 5F′) detected in an additional ~25% of cells. Although ultrastructural analysis would be required to definitively show the ladder-like organization of septate junctions, we find that costaining experiments (Figure S3) for Vari and Fas3 showed identical or largely overlapping distribution in 100% of cells (n = 17), suggesting the maintenance of functional septate junctions in the transition zone. Furthermore, we found that septate junction proteins were present in foci far from the transition zone (Figures 5G and 5G′); these foci showed only partial costaining for Fas3 and Vari. The ectopic puncta of junctional protein may represent protein undergoing vesicular trafficking; Tiklová et al. (2010) show that dispersed basolateral septate junction proteins are trafficked through an endocytic pathway prior to their assembly in mature septate junctions. However, we were unable to detect substantial colocalization between isolated Fas3 puncta and Lamp-1, FYVE-GFP, Rab4, 5, or 11 (Figure S3). These data suggest that ectopic Fas3 may be present at the basolateral membrane at steady state, perhaps reflecting a deficit in endocytosis or in the initial targeting of Fas3 containing vesicles. Similar defects were seen for septate junctions in *Ccm3* RNAi animals (Figure S3). In contrast, septate junctions appeared largely similar to wild-type in *lotus* terminal cells (Figure S4). Because it has been suggested that autocellular tubes in the terminal cell transition zone may derive from the neighboring stalk cell, which might insert its tube into the terminal cell like a finger poking into a balloon (Uv et al., 2003), we tested whether the septate junctions we detect are autonomous to the terminal cell, and found that they are (Figure S3).

In previous work (Schottenfeld-Roames and Ghabrial, 2012), we found that Crumbs-GFP expressed as a functional knockin allele (Huang et al., 2009), is detected in discrete puncta throughout the membrane that surrounds the lumen of seamless tubes in terminal cells (Figure 5H). In a second study, we determined that a mutation causing multiple seamless tube microdilations was associated with overaccumulation of Crumbs on the lumenal membrane (Schottenfeld-Roames and A.S.G., unpublished data). We note that multiple microdilations can be detected in *wheezy* terminal cells upon staining with an apical membrane marker (also observed with *Ccm3* RNAi; Figure S1). This led us to explore whether elevated Crumbs levels might also be involved in the *wheezy* and *Ccm3* transition zone dilations. In terminal cells depleted of GCKIII by RNAi, Crumbs-GFP levels were dramatically increased (Figure 5I), and the protein accumulated more uniformly along the lumenal membrane (compare Figures 5J and 5K). In contrast, we noted that in *lotus* mutant cells, Crumbs accumulated to high levels but was no longer restricted to the lumenal membrane (Figure 5L). In double mutants, we observed that *lotus* was epistatic to *wheezy*, consistent with the possibility that apical Crumbs accumulation may be required for tube dilation (Figures 6A–6C)—in the double mutant, Crumbs localization was as in *lotus* single mutants (Figure S5). As might be expected, in ~70% of terminal cells (9/13) no tube was present in the transition zone as a consequence of loss of *lotus* (Figure 6C; apical membrane staining not shown); however, in the remaining 30% of cells (4/13) with a continuous transition zone tube we observed suppression of the *wheezy* tube dilation (Movie S1).

Depletion of *crumbs* Suppresses the *wheezy* Tube Dilation Phenotype

Importantly, overexpression of Crumbs by itself does not give rise to the large transition zone dilation observed in *wheezy* mutant terminal cells (Schottenfeld-Roames and A.S.G., unpublished data); however, we wondered if, as suggested by the *lotus-wheezy* epistasis results, it might nevertheless contribute to the transition zone tube dilations. We asked if Crumbs depletion might suppress the transition zone dilation defect in *wheezy* mutant cells. We found that knockdown of *crumbs* by RNAi in *wheezy* mutant terminal cells completely suppressed the transition zone dilation defect (Figure 6F) in 61% of terminal cells and appeared to reduce the severity of the dilation in an additional 27% of cells (n = 55). These data imply that apical accumulation of Crumbs is required for the dilations observed in *wheezy* mutants, but is not in itself sufficient to cause them. The mechanism responsible for Crumbs accumulation in *wheezy* mutant cells is not yet clear; however, we have found a substantial enrichment of Rab11 within the transition zone, associated with dilated tube (59% of terminal cells, n = 32; Figures 6D and 6E). This suggests that GCKIII affects the spatial distribution of the recycling endosome compartment, and may regulate Crb levels via vesicular trafficking.

Depletion of *varicose* Suppresses the *wheezy* Tube Dilation Phenotype

We next asked whether the increase in septate junctions in *wheezy* mutants contributed to the transition zone dilation defect. To do so, we tested whether depletion of Varicose, a MAGUK protein required for septate junction assembly and function (Bachmann et al., 2008; Moyer and Jacobs, 2008; Wu et al., 2007), was able to suppress the *wheezy* tube dilation defect. We found that transition zone tube dilation was completely suppressed in 52% of terminal cells and partially suppressed in another 20%, whereas an additional 9% of cells actually showed the discontinuous tube (“gap”) defect characteristic of *lotus* (n = 48) (Figure 6F). That knockdown of *varicose* in a *wheezy* mutant background can give rise to the full spectrum of transition zone tube phenotypes suggests that the effects of knockdown are dosage sensitive. Consistent with a dosage sensitivity for *varicose*, we note that the Leptin lab was unable to recover homozygous mutant tracheal cell clones deficient for *varicose* (Baer et al., 2007). Under the RNAi conditions we used, depletion of *varicose* in an otherwise wild-type background did not cause an obvious tubulogenesis defect, although we could observe altered localization of Fas3 (Figure S6). We interpret these results as implicating septate junctions in targeting of membrane addition to the transition zone tube. Strikingly, in *wheezy* terminal cells in which *varicose* knockdown suppressed the transition zone dilation, the presence and number of seamless tube microdilations was not altered (Table S2); this implies that the large dilations resulting from loss of *wheezy* function reflect a specific transition zone requirement for GCKIII.

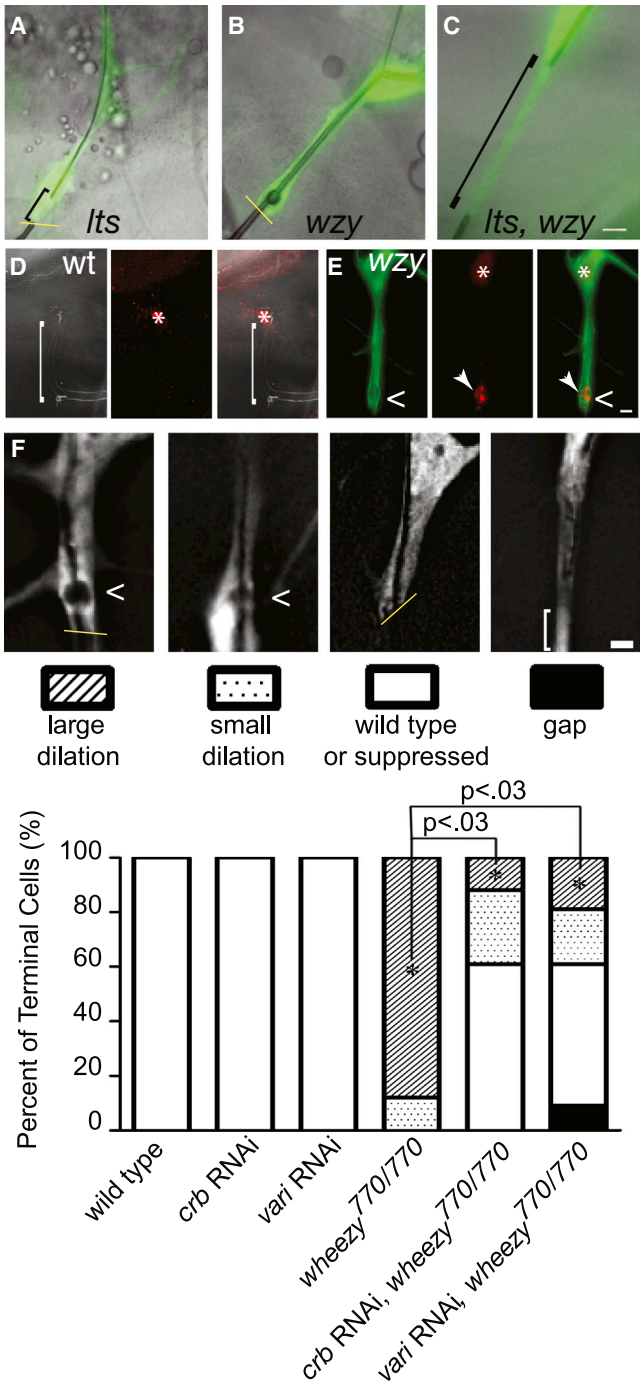

Figure 6. Genetic Suppression of *wheezy* Transition Zone Tube Dilations

In epistasis experiments, we found that *lotus*, *wheezy* double mutant terminal cell clones (C, compare to single mutant cells in A and B) show the *lotus* mutant phenotype, perhaps because Crumbs protein is mislocalized in the double mutant cells (Figure S5). Staining of endogenous Rab11 in wild-type (D) and *wheezy* mutant (E) terminal cells suggests that there is a dramatic enrichment of Rab11 in the transition zone upon loss of GCKIII activity. Mosaic animals were generated and the homozygous mutant *wheezy* clone (E) is marked with GFP (green), whereas neighboring heterozygous control terminal cells are GFP negative (D). In heterozygous control cells, tube lumens were visualized by autofluorescence in the UV channel (white), and the transition zone is indicated by (|). Control terminal cells were identified by nuclear DsRED2 expression and by tube morphology. Dilation indicated by < , nucleus by *, and Rab11 by arrowhead. To directly test whether knockdown of *crumbs*, or of septate junctions, could suppress the transition zone tube dilation defect of *wheezy*, we carried out similar epistasis experiments. Terminal cell transition zone tubes were classified into one of four categories (F): large dilation, indicating no modification of the *wheezy* tube dilation defect; small dilation, indicating a partial suppression of the defect, wild-type or suppressed—indicating no dilation or a complete suppression of the transition zone dilation; and gap, indicating a discontinuous tube defect similar to that seen in *lotus* terminal cells. Dilations are indicated by < ; the terminal cell stalk cell interfaces (if within field of view) are indicated by a yellow line; and the extent of the transition zone tube gap is indicated by a bracket. Genotypes of terminal cell clones shown in (F) are (left to right): $wheezy^{770/770}$; $wheezy^{770/770}$ with RNAi knockdown of *crumbs*; $wheezy^{770/770}$ with RNAi knockdown of *crumbs*; $wheezy^{770/770}$ with RNAi knockdown of *varicose*. Expression of *crb* or *vari* RNAi in wild-type terminal cells with the *btl*-GAL4 driver at 25°C did not alter the normal morphology of transition zone tubes, but their expression in *wheezy* mutant cells dramatically suppressed the dilation defect (F). To compare *wheezy* clones to *wheezy* clones with *crumbs* or *varicose* RNAi, a p value was calculated using a two-tailed Student's t test. The fraction of transition zone tubes with large dilations was scored, and the mean of the three trials was used. For the histogram plotted in (E), the total number of terminal cells scored were as follows: n = 25 (WT); 41 (*crb* RNAi); 38 (*vari* RNAi); 51 ($wheezy^{770}$ clones); 55 $wheezy^{770}$ clones with *crb* RNAi), and 48 ($wheezy^{770}$ clones with *vari* RNAi). All images depict third instar larvae. Scale bars represent 5 μm.
See also Figure S6 and Movie S1.

DISCUSSION

In the terminal cell "transition zone," seamed and seamless tubes must connect. We found that during development, remodeling of cell junctions reduced tube type complexity in the transition zone, such that by third instar only seamless tubes are still present in the majority of terminal cells. How the tubes connect initially has been an outstanding question in the field for more than a decade, and whether, or how, transition zone tubes remodel over developmental time has not previously been addressed. In this manuscript, we describe several mutations that disrupt tube morphogenesis in the terminal cell transition zone. The mutants fall into two classes that appear to act in opposing manners: in the case of mutants like *lotus*, there appears to be a deficit of apical membrane addition to the growing tube within the transition zone, most frequently resulting in a failure to maintain a continuous tube. In the case of mutants such as *wheezy*, too much apical membrane is added to the transition zone tube, resulting in a grossly dilated appearance. Our molecular genetic characterization of the genes is consistent with this hypothesis as *lotus* encodes a factor required for membrane traffic and *wheezy* encodes a putative Golgi-resident kinase that we show is required for restricting the accumulation of apical and junctional proteins. In this context, it is important to consider that secretion of specific cargo into the tube lumen during embryonic tracheal development is dependent upon septate junctions (Wang et al., 2006); perhaps an increase in transition zone septate junctions promotes enhanced targeting of vesicles to the lumenal membrane. However, the existence of septate junctions in the transition zone by itself does not appear to lead to tube dilation because ~4% of wild-type third instar terminal cells have septate junctions in the transition zone, but do not have dilations. This, together with the inability of Crumbs overexpression to cause transition zone dilations,

and with the suppression of such dilations by knockdown of *crumbs* or of *varicose*, leads us to propose that both ectopic septate junctions and increased accumulation of apical polarity proteins are required for transition zone tube dilation. Our study provides genetic and molecular insight into the process of junctional remodeling and tubulogenesis in the transition zone.

We have determined that *wheezy* encodes GCKIII, the only known downstream effector of CCM3, a protein mutated in human vascular disease characterized by grossly dilated, leaky capillaries. It therefore becomes important to ask whether our insights into the cellular basis of GCKIII/CCM3 deficiency are compatible with what is known from patient samples and vertebrate CCM models. In excised CCMs, staining of apical polarity proteins and junctional proteins has not been reported, but ultrastructural analyses suggest that endothelial cells lack functional tight junctions, and in mouse models, lymphatic vessels show gaps between endothelial cells or show shorter intercellular junctions (Clatterbuck et al., 2001; Kleaveland et al., 2009). On the other hand, EM analysis of vessels from endothelial-specific *Ccm3* knockout mice showed tight junctions were present and did not detect any gaps between endothelial cells (Chan et al., 2011). It is not clear how to reconcile these data, although it is possible that loss of CCM1 and CCM2 cause tube dilation by a mechanism that is distinct from that seen with loss of CCM3, as suggested by Chan et al. (2011). In the *Drosophila* tracheal system, we see a clear and dramatic increase in apical polarity protein accumulation, and a convincing defect in remodeling of septate junctions; this suggests that a reexamination of endothelial tight junctions and an initial study of apical polarity determinants in vertebrate CCM models should be a high priority. Indeed, extant data hint that such studies could be of great value. For example, mutations in the zebrafish orthologs of Stardust and Yurt (physical interactors and regulators of Crumbs in *Drosophila*) have cardiovascular defects (Jensen et al., 2001; Jensen and Westerfield, 2004). Moreover, remodeling of endothelial cell junctions during angiogenesis, as cells change neighbors and as the tubes they comprise change architectures, is likely to be critical to the formation of functional tubes. That terminal cells are the only tracheal cell type affected by loss of CCM3 or GCKIII activity is striking, and may be directly relevant to human disease given that ~30% of cells comprising capillaries in the cerebral cortex have an analogous cellular architecture, the so-called "seamless" endothelial cells (Bär et al., 1984). In addition, we note that the cellular architecture of endothelial tip cells that lead outgrowth of the zebrafish intersomitic vessels is dynamic: these cells often form seamless tubes, but sometimes appear to make tubes of mixed autocellular and seamless character (like fly terminal cells), and at other times appear to contribute to multicellular tubes (Blum et al., 2008; Herwig et al., 2011). Given the dynamic nature of tight junctions during angiogenesis, defects in junction remodeling such as those we see with *wheezy* mutants in the *Drosophila* tracheal system, might be expected to give rise to leaky vessels composed of endothelial cells that are not properly attached to each other.

The precise function of CCM3 and GCKIII during angiogenesis is not clear. Recently Chan et al. (2011) have suggested a requirement for the CCM3 pathway in lumen formation, whereas Zheng et al. (2010) have suggested that the pathway regulates cell junctions via phosphorylation of Moesin. Our data conclusively show that neither model is consistent with the observed effects of loss of the CCM3/GCKIII pathway in the fly tracheal system; we discuss each model in the context of our data below.

The lumen formation model of Chan et al. (2011) is built upon the outcome of two sets of experiments: tubulogenesis assays of CCM3- or GCKIII-depleted endothelial cells and RNAi studies in the *Drosophila* tracheal system. The tubulogenesis assays have been used to great effect by Bayless et al. (2000), Fisher et al. (2009, and Koh et al. (2009), allowing them to identify a number of genes required for endothelial lumen formation; however, it is important to appreciate that the endothelial cells in this assay must do more than simply lumenize, they must also migrate, remodel the matrix, and organize and reorganize cell:cell contacts. Disruption in any of these preconditions for lumenization would also compromise tubulogenesis. Thus, should the junctional remodeling defects observed in the fly tracheal system also pertain to endothelial cells depleted for CCM3 or GCKIII, those remodeling defects might be sufficient to block lumenization in the in vitro assays. Additionally, the fact that patient CCMs are dilated capillaries rather than lumenless capillaries would also seem to argue against this model.

We note that our data for *GckIII* and *Ccm3* in the *Drosophila* tracheal system stand in contrast to the findings of Chan et al. (2011). Unlike Chan et al. (2011), we find tube dilation to be the primary consequence of loss of CCM3 or GCKIII function. The fully penetrant transition zone defect we observed in *wheezy* mutant flies is compelling, and is directly supported, in our hands, by RNAi experiments targeting either *GckIII* or *Ccm3*, including with RNAi transgenes employed by Chan et al. (2011) (Table S1). Consistent with the findings of Chan et al. (2011), we do observe defects in terminal cell gas-filling (but not in other tracheal cell tubes by mosaic analysis using a null allele of *GckIII*). However, we find that the lack of observable gas-filled tubes is not due to failure in tube formation, as suggested by Chan et al. (2011), but rather due to a failure in liquid clearance. Indeed, we readily detected liquid-filled tubes in the knocked-down cells (Figure S1). Importantly, our data argue that *Ccm3* and *GckIII* are not required for making a lumen, but instead are required to prevent inappropriate trafficking of junctional and apical proteins.

We have also addressed the Zheng et al. (2010) model that phosphorylation of Moesin is the essential function of the CCM3/GCKIII pathway during tubulogenesis. Moesin is the only ERM (ezrin-radixin-moesin) family member in *Drosophila*, and we find that phosphorylation of Moesin in the tracheal system is not compromised by loss of CCM3 or GCKIII (in fact it is elevated). These data suggest that the essential target of GCKIII kinase activity is not Moesin, but another protein yet to be identified. Going forward, it will be of great interest to determine what proteins are regulated by GCKIII kinase activity in the tracheal system, and to test whether vertebrate orthologs of these factors are required during angiogenesis.

EXPERIMENTAL PROCEDURES

Fly Strains

lotus^{312}, *urdur*^{2}, and *wheezy*^{770} alleles were described (Ghabrial et al., 2011; Kennison and Tamkun, 1988). *lotus*^{O48} and *lotus*^{B91} were isolated in an EMS mutagenesis screen (below). Tissue-specific knockdown was with the GAL4/UAS system. Driver lines used were *btl-GAL4* (pan-tracheal) and *srf-GAL4* (terminal cell; a gift from Mark Metzstein); and RNAi responder strains

were VDRC939 (Fas3), VDRC7743 (*Nsf2*), VDRC49559, VDRC49558, VDRC107158 (*GckIII*), VDRC46548, VDRC106841, VDRC109453 (*Ccm3*), VDRC24157 (*varicose*), and VDRC39177 (*crumbs*). A full-length cDNA of *GckIII* was cloned into pUAST using EcoRI and KpnI, and transgenic flies were generated (Genetic Services). In rescue experiments *UAS-GCKIII* was driven by *btl-GAL4*. UAS-GFP-Lamp1 was a gift from Helmut Kramer. The *crumbs-GFPA* stock was a gift from Yong Hong (Huang et al., 2009). UAS-YFP-Rab4, UAS-YFP-Rab5, UAS-GFP-myc2xFYVE, *urdur*^{2}, P{EPg} CG5073^{HP36555}, and deficiency strains were obtained from the Bloomington *Drosophila* Stock Center.

Allele Screens

Additional alleles of *lotus* were isolated in an EMS mutagenesis screen. *btl* > GFP; FRT^{2A}, FRT^{82B} males were mutagenized, and ~2,000 F1 males with lethal mutations were generated. Alleles of *lotus* were identified using a *lotus*^{312} tester strain, and validated by tracheal phenotype.

Generation of CCM3 Excision Alleles

Male P{EPg}CG5073^{HP36555} flies were crossed with virgins carrying Δ2–3 transposase. Two hundred independently derived chromosomes were recovered that had lost the w^{+} minigene marking the P element; these were balanced over TM3, *Sb*. Precise and imprecise excision alleles was identified by complementation test with Df(3R)EXEL6174, and by sequence analysis. The presence of at least two lethal mutations on the right arm of chromosome 3 in the P{EPg}CG5073^{HP36555} stock precluded their use in analysis of homozygous mutant animals. Primers pairs used for PCR amplification and sequencing were: 5′-ATGGACTTCTGGTCGGTGAG-3′, and 5′-AATCGCAA CTGGGTTCCTGC-3′; 5′-CAATCGTAAGTCCGTGGCTCTC-3′, and 5′-TCGT CCGTCTCCATAAATAGTTGC-3′; 5′-TCCAAGAAGTTCAGCACAACGC-3′, and 5′-AAAAGTGGGTCATCTCGGTCG-3′.

Mosaic Analysis

Virgin *hsFLP*^{122}; *btl*-GAL4 UAS-GFP, or UAS-DsRed; FRT^{82B} Tub-GAL80 (Lee and Luo, 2001) or UAS-GFP RNAi (Ghabrial et al., 2011) flies were crossed to males bearing the mutation of interest on an FRT^{82B} chromosome. Embryos were collected 0–4 hr after egg lay, and subjected to a 38°C heat shock for 45–55 min to induce expression of FLP recombinase, and then allowed to develop at 25°C until third larval instar (L3). For *wheezy* clones in which *Fas3* was knocked down by RNAi: virgin hsFLP^{122}; UAS-*Fas3*RNAi; FRT^{82B}, Tub-GAL80 flies were crossed to male *btl-GAL4*, UAS-GFP; FRT^{2A},FRT^{82B}, *wheezy*^{770}/TM3*Sb*, Tub-GAL80. For *wheezy* clones with pan-tracheal *varicose* knockdown: virgin hsFLP^{122}; UAS-*vari*RNAi; FRT^{2A},FRT^{82B}, *wheezy*^{770}/ TM3*Sb*, Tub-GAL80 flies were crossed to male *btl-GAL4*, UAS-GFP; FRT^{82B}, *cu*, UAS-GFP-RNAi flies. Larvae were mounted in 60% glycerol, killed by heating on a 70°C block for ~10 s, and examined with a Leica fluorescence microscope, or were filleted ventrally in ice cold PBS and processed for antibody staining as described below.

Sequence Analysis

lotus, *urdur*, or *wheezy* alleles were balanced over TM3, *Sb*, *Ser*, *twi-GAL4*, UAS-GFP (Bloomington). Homozygous mutant embryos were selected, and DNA was extracted using QIAamp DNA Mini Kit (QIAGEN). Amplicons covering all exons and splice sites were and sequenced. *Nsf2* primers were: TACA CACACGCAATGCCGAACAGG and TCTCACTACCGCTATGCTATGAACG; GGTTCTCGGTTTATCTCGGACG and TGGCTTCTGATTCACCCACG; CCT CGCTGTAAAAACGCTGG and AAAGTCACGCATCCGCTTGGTGTG; GAGTT CAATGCGATTTTCCGAC, and GCAGTTTTTCCATAGCCTCCG; CCAGTTGA GTGATTTCCCATTCG, and CGGTTCTGTGTATTAGGCTTGAAGG; CAAA GAACTTCAGTGGCG-, and GCGGTTGCTTTTTCAGTAG. *GckIII* primers were: CTTTTCGGAACTGCTAACG and CCATAACTTGGTGCCCTT; GGAG TAACAAGGAAACCCG and GGGTGGATTGTTCTTGGGGA; AAGGGCGAC GAAAGTGAGAC and CGTTTCAGTTTGTGTTGTCTCG; GAACAACTTCCT CTTCCCC and GGGTTCCTCATTTCCAATAAGG. For *lotus*^{312}, a single nucleotide change was detected corresponding to a T-to-A transition, which caused an amino acid substitution in the conserved N domain of NSF2; for the *lotus*^{B91}, a G-to-C nucleotide change was detected that caused a missense mutation in the conserved D1 domain of NSF2; for *lotus*^{O48}, a G-to-A transition was detected, that caused a nonsense mutation at the 75th codon of *Nsf2*. In *urdur*^{2}, a G-to-A mutation affecting the splice donor site of the second exon of *NSF2* was detected. In *wheezy*^{770}, a C-to-T transition caused a nonsense mutation in codon 57 of *GckIII*.

Penetrance of Tube Dilation Defects

To compare among different genotypes, dorsal branch terminal cells from L3 larvae were scored. All dorsal branch terminal cells (~20) in five larvae were scored in each of three trials.

Immunohistochemistry

L3 larvae were dissected and fixed as described (Schottenfeld-Roames and Ghabrial, 2012). Primary antibody incubations were at 4°C overnight. Primary antibodies used were mouse α-Fas3 (DSHB; 1:50), mouse α-Coracle (DSHB, a cocktail of C566.9C and C615.16A, each at1:500), rabbit α-Rab11 (a gift from Robert Cohen, 1:500), rabbit α-Varicose (a gift from Elisabeth Knust; 1:500), Chicken α-GFP (Invitrogen;1:500), Mouse-α-Phospho-ERM (Cell Signaling; 1:200), mouse α-RFP (Abcam; 1:1,000), and rabbit α-Wkd (Schottenfeld-Roames and Ghabrial, 2012). Secondary antibody incubations were at room temperature for 1 hr. Alexa Fluor 488, 555, and 647 conjugated secondary antibodies were used (Invitrogen; 1:1,000). Samples were mounted in aquapolymount (Polysciences), and images were acquired on a Leica DM5500 compound microscope. Z stacks were captured for most images. Where possible, single z images are shown. When deemed necessary for clarity, optimal focal planes (planes that bisect the tube) were merged to generate a montage of different z series in the same x,y position—images that are montages are indicated in the legends for Figures 1, 2, 3, 5, S1, S2, S3, S4, S5, and S6.

Statistical Analysis

varicose and *crumbs* knockdown experiments were done in the background of *wheezy* or wild-type control mosaic larvae. No knockdown, or pan-tracheal knockdown using *crumbs* or *varicose* RNAi, was driven by *breathless*-GAL4 For each group (wild-type 3R clone, no RNAi; wild-type 3R clone, *crumbs* RNAi; wild-type 3R clone, *varicose* RNAi; *wheezy* clone, no RNAi; *wheezy* clone, *crumbs* RNAi; *wheezy* clone, *varicose* RNAi), experiments were set up simultaneously in triplicate and the transition zone tube phenotype of all clones were scored (large dilation, small dilation, wild-type/suppressed dilation, or gap). The fraction of transition zone tubes with large dilations was determined, and the mean of the three trials was used to calculate a p value by a two-tailed Student's t test, comparing *wheezy* clones to *wheezy* clones with *crumbs* or *varicose* RNAi.

SUPPLEMENTAL INFORMATION

Supplemental Information includes six figures, two tables, and one movie and can be found with this article online at http://dx.doi.org/10.1016/j.devcel.2013.05.002.

ACKNOWLEDGMENTS

We thank Drs. Steve DiNardo, Mark Kahn, and Meera Sundarum, the members of the Ghabrial laboratory, and three anonymous reviewers for their comments on the manuscript. A.S.G. gratefully acknowledges support from the University of Pennsylvania and the NIH (1R01GM089782-01A1). This work was supported in part by Basil O'Connor Starter Scholar Research Award Grant No. 5-FY09-43 from the March of Dimes Foundation.

Received: November 27, 2012
Revised: April 9, 2013
Accepted: May 2, 2013
Published: June 10, 2013

REFERENCES

Bachmann, A., Draga, M., Grawe, F., and Knust, E. (2008). On the role of the MAGUK proteins encoded by Drosophila varicose during embryonic and postembryonic development. BMC Dev. Biol. *8*, 55.

Baer, M.M., Bilstein, A., and Leptin, M. (2007). A clonal genetic screen for mutants causing defects in larval tracheal morphogenesis in Drosophila. Genetics *176*, 2279–2291.

Bär, T., Güldner, F.H., and Wolff, J.R. (1984). "Seamless" endothelial cells of blood capillaries. Cell Tissue Res. *235*, 99–106.

Bayless, K.J., Salazar, R., and Davis, G.E. (2000). RGD-dependent vacuolation and lumen formation observed during endothelial cell morphogenesis in three-dimensional fibrin matrices involves the alpha(v)beta(3) and alpha(5)beta(1) integrins. Am. J. Pathol. *156*, 1673–1683.

Bergametti, F., Denier, C., Labauge, P., Arnoult, M., Boetto, S., Clanet, M., Coubes, P., Echenne, B., Ibrahim, R., Irthum, B., et al.; Société Française de Neurochirurgie. (2005). Mutations within the programmed cell death 10 gene cause cerebral cavernous malformations. Am. J. Hum. Genet. *76*, 42–51.

Blum, Y., Belting, H.G., Ellertsdottir, E., Herwig, L., Lüders, F., and Affolter, M. (2008). Complex cell rearrangements during intersegmental vessel sprouting and vessel fusion in the zebrafish embryo. Dev. Biol. *316*, 312–322.

Chan, A.C., Drakos, S.G., Ruiz, O.E., Smith, A.C., Gibson, C.C., Ling, J., Passi, S.F., Stratman, A.N., Sacharidou, A., Revelo, M.P., et al. (2011). Mutations in 2 distinct genetic pathways result in cerebral cavernous malformations in mice. J. Clin. Invest. *121*, 1871–1881.

Clatterbuck, R.E., Eberhart, C.G., Crain, B.J., and Rigamonti, D. (2001). Ultrastructural and immunocytochemical evidence that an incompetent blood-brain barrier is related to the pathophysiology of cavernous malformations. J. Neurol. Neurosurg. Psychiatry *71*, 188–192.

Fidalgo, M., Fraile, M., Pires, A., Force, T., Pombo, C., and Zalvide, J. (2010). CCM3/PDCD10 stabilizes GCKIII proteins to promote Golgi assembly and cell orientation. J. Cell Sci. *123*, 1274–1284.

Fisher, K.E., Sacharidou, A., Stratman, A.N., Mayo, A.M., Fisher, S.B., Mahan, R.D., Davis, M.J., and Davis, G.E. (2009). MT1-MMP- and Cdc42-dependent signaling co-regulate cell invasion and tunnel formation in 3D collagen matrices. J. Cell Sci. *122*, 4558–4569.

Gervais, L., and Casanova, J. (2010). In vivo coupling of cell elongation and lumen formation in a single cell. Curr. Biol. *20*, 359–366.

Gervais, L., Lebreton, G., and Casanova, J. (2012). The making of a fusion branch in the Drosophila trachea. Dev. Biol. *362*, 187–193.

Ghabrial, A.S., and Krasnow, M.A. (2006). Social interactions among epithelial cells during tracheal branching morphogenesis. Nature *441*, 746–749.

Ghabrial, A.S., Levi, B.P., and Krasnow, M.A. (2011). A systematic screen for tube morphogenesis and branching genes in the Drosophila tracheal system. PLoS Genet. *7*, e1002087.

Golby, J.A., Tolar, L.A., and Pallanck, L. (2001). Partitioning of N-ethylmaleimide-sensitive fusion (NSF) protein function in Drosophila melanogaster: dNSF1 is required in the nervous system, and dNSF2 is required in mesoderm. Genetics *158*, 265–278.

Guclu, B., Ozturk, A.K., Pricola, K.L., Bilguvar, K., Shin, D., O'Roak, B.J., and Gunel, M. (2005). Mutations in apoptosis-related gene, PDCD10, cause cerebral cavernous malformation 3. Neurosurgery *57*, 1008–1013.

Haasdijk, R.A., Cheng, C., Maat-Kievit, A.J., and Duckers, H.J. (2012). Cerebral cavernous malformations: from molecular pathogenesis to genetic counselling and clinical management. Eur. J. Hum. Genet. *20*, 134–140.

He, Y., Zhang, H., Yu, L., Gunel, M., Boggon, T.J., Chen, H., and Min, W. (2010). Stabilization of VEGFR2 signaling by cerebral cavernous malformation 3 is critical for vascular development. Sci. Signal. *3*, ra26.

Herwig, L., Blum, Y., Krudewig, A., Ellertsdottir, E., Lenard, A., Belting, H.G., and Affolter, M. (2011). Distinct cellular mechanisms of blood vessel fusion in the zebrafish embryo. Curr. Biol. *21*, 1942–1948.

Huang, J., Zhou, W., Dong, W., Watson, A.M., and Hong, Y. (2009). From the cover: directed, efficient, and versatile modifications of the Drosophila genome by genomic engineering. Proc. Natl. Acad. Sci. USA *106*, 8284–8289.

Hughes, S.C., Formstecher, E., and Fehon, R.G. (2010). Sip1, the Drosophila orthologue of EBP50/NHERF1, functions with the sterile 20 family kinase Slik to regulate Moesin activity. J. Cell Sci. *123*, 1099–1107.

Ikeya, T., and Hayashi, S. (1999). Interplay of Notch and FGF signaling restricts cell fate and MAPK activation in the Drosophila trachea. Development *126*, 4455–4463.

Jensen, A.M., and Westerfield, M. (2004). Zebrafish mosaic eyes is a novel FERM protein required for retinal lamination and retinal pigmented epithelial tight junction formation. Curr. Biol. *14*, 711–717.

Jensen, A.M., Walker, C., and Westerfield, M. (2001). mosaic eyes: a zebrafish gene required in pigmented epithelium for apical localization of retinal cell division and lamination. Development *128*, 95–105.

Kennison, J.A., and Tamkun, J.W. (1988). Dosage-dependent modifiers of polycomb and antennapedia mutations in Drosophila. Proc. Natl. Acad. Sci. USA *85*, 8136–8140.

Kleaveland, B., Zheng, X., Liu, J.J., Blum, Y., Tung, J.J., Zou, Z., Sweeney, S.M., Chen, M., Guo, L., Lu, M.M., et al. (2009). Regulation of cardiovascular development and integrity by the heart of glass-cerebral cavernous malformation protein pathway. Nat. Med. *15*, 169–176.

Koh, W., Sachidanandam, K., Stratman, A.N., Sacharidou, A., Mayo, A.M., Murphy, E.A., Cheresh, D.A., and Davis, G.E. (2009). Formation of endothelial lumens requires a coordinated PKCepsilon-, Src-, Pak- and Raf-kinase-dependent signaling cascade downstream of Cdc42 activation. J. Cell Sci. *122*, 1812–1822.

Lee, S., and Kolodziej, P.A. (2002). The plakin Short Stop and the RhoA GTPase are required for E-cadherin-dependent apical surface remodeling during tracheal tube fusion. Development *129*, 1509–1520.

Lee, S.T., Choi, K.W., Yeo, H.T., Kim, J.W., Ki, C.S., and Cho, Y.D. (2008). Identification of an Arg35X mutation in the PDCD10 gene in a patient with cerebral and multiple spinal cavernous malformations. J. Neurol. Sci. *267*, 177–181.

Lee, T., and Luo, L. (2001). Mosaic analysis with a repressible cell marker (MARCM) for Drosophila neural development. Trends Neurosci. *24*, 251–254.

Llimargas, M. (1999). The Notch pathway helps to pattern the tips of the Drosophila tracheal branches by selecting cell fates. Development *126*, 2355–2364.

Lubarsky, B., and Krasnow, M.A. (2003). Tube morphogenesis: making and shaping biological tubes. Cell *112*, 19–28.

Moyer, K.E., and Jacobs, J.R. (2008). Varicose: a MAGUK required for the maturation and function of Drosophila septate junctions. BMC Dev. Biol. *8*, 99.

Pagenstecher, A., Stahl, S., Sure, U., and Felbor, U. (2009). A two-hit mechanism causes cerebral cavernous malformations: complete inactivation of CCM1, CCM2 or CCM3 in affected endothelial cells. Hum. Mol. Genet. *18*, 911–918.

Preisinger, C., Short, B., De Corte, V., Bruyneel, E., Haas, A., Kopajtich, R., Gettemans, J., and Barr, F.A. (2004). YSK1 is activated by the Golgi matrix protein GM130 and plays a role in cell migration through its substrate 14-3-3zeta. J. Cell Biol. *164*, 1009–1020.

Rasmussen, J.P., English, K., Tenlen, J.R., and Priess, J.R. (2008). Notch signaling and morphogenesis of single-cell tubes in the C. elegans digestive tract. Dev. Cell *14*, 559–569.

Ribeiro, C., Neumann, M., and Affolter, M. (2004). Genetic control of cell intercalation during tracheal morphogenesis in Drosophila. Curr. Biol. *14*, 2197–2207.

Rigamonti, D., Hadley, M.N., Drayer, B.P., Johnson, P.C., Hoenig-Rigamonti, K., Knight, J.T., and Spetzler, R.F. (1988). Cerebral cavernous malformations. Incidence and familial occurrence. N. Engl. J. Med. *319*, 343–347.

Samakovlis, C., Hacohen, N., Manning, G., Sutherland, D.C., Guillemin, K., and Krasnow, M.A. (1996a). Development of the Drosophila tracheal system occurs by a series of morphologically distinct but genetically coupled branching events. Development *122*, 1395–1407.

Samakovlis, C., Manning, G., Steneberg, P., Hacohen, N., Cantera, R., and Krasnow, M.A. (1996b). Genetic control of epithelial tube fusion during Drosophila tracheal development. Development *122*, 3531–3536.

Sanyal, S., and Krishnan, K.S. (2001). Lethal comatose mutation in Drosophila reveals possible role for NSF in neurogenesis. Neuroreport *12*, 1363–1366.

Schottenfeld-Roames, J., and Ghabrial, A.S. (2012). Whacked and Rab35 polarize dynein-motor-complex-dependent seamless tube growth. Nat. Cell Biol. *14*, 386–393.

Stone, C.E., Hall, D.H., and Sundaram, M.V. (2009). Lipocalin signaling controls unicellular tube development in the Caenorhabditis elegans excretory system. Dev. Biol. *329*, 201–211.

Sutherland, D., Samakovlis, C., and Krasnow, M.A. (1996). branchless encodes a Drosophila FGF homolog that controls tracheal cell migration and the pattern of branching. Cell *87*, 1091–1101.

Tiklová, K., Senti, K.A., Wang, S., Gräslund, A., and Samakovlis, C. (2010). Epithelial septate junction assembly relies on melanotransferrin iron binding and endocytosis in Drosophila. Nat. Cell Biol. *12*, 1071–1077.

Tsarouhas, V., Senti, K.A., Jayaram, S.A., Tiklová, K., Hemphälä, J., Adler, J., and Samakovlis, C. (2007). Sequential pulses of apical epithelial secretion and endocytosis drive airway maturation in Drosophila. Dev. Cell *13*, 214–225.

Uv, A., Cantera, R., and Samakovlis, C. (2003). Drosophila tracheal morphogenesis: intricate cellular solutions to basic plumbing problems. Trends Cell Biol. *13*, 301–309.

Voss, K., Stahl, S., Hogan, B.M., Reinders, J., Schleider, E., Schulte-Merker, S., and Felbor, U. (2009). Functional analyses of human and zebrafish 18-amino acid in-frame deletion pave the way for domain mapping of the cerebral cavernous malformation 3 protein. Hum. Mutat. *30*, 1003–1011.

Wang, S., Jayaram, S.A., Hemphälä, J., Senti, K.A., Tsarouhas, V., Jin, H., and Samakovlis, C. (2006). Septate-junction-dependent luminal deposition of chitin deacetylases restricts tube elongation in the Drosophila trachea. Curr. Biol. *16*, 180–185.

Wu, V.M., Yu, M.H., Paik, R., Banerjee, S., Liang, Z., Paul, S.M., Bhat, M.A., and Beitel, G.J. (2007). Drosophila Varicose, a member of a new subgroup of basolateral MAGUKs, is required for septate junctions and tracheal morphogenesis. Development *134*, 999–1009.

Zhao, C., Smith, E.C., and Whiteheart, S.W. (2012). Requirements for the catalytic cycle of the N-ethylmaleimide-Sensitive Factor (NSF). Biochim. Biophys. Acta *1823*, 159–171.

Zheng, X., Xu, C., Di Lorenzo, A., Kleaveland, B., Zou, Z., Seiler, C., Chen, M., Cheng, L., Xiao, J., He, J., et al. (2010). CCM3 signaling through sterile 20-like kinases plays an essential role during zebrafish cardiovascular development and cerebral cavernous malformations. J. Clin. Invest. *120*, 2795–2804.